

A Deeper Investigation of the Primordial Binary Cluster Candidate

QINGSHUN HU,¹ YUTING LI,¹ MINGFENG QIN,^{2,3} CHENGLONG LV,⁴ YANG PAN,¹ AND YANGPING LUO¹

¹*School of Physics and Astronomy, China West Normal University, No. 1 Shida Road, Nanchong 637002, People's Republic of China*

²*Institute for Frontiers in Astronomy and Astrophysics, Beijing Normal University, Beijing 102206, People's Republic of China*

³*School of Physics and Astronomy, Beijing Normal University, Beijing 100875, People's Republic of China*

⁴*Xinjiang Astronomical Observatory, Chinese Academy of Sciences, No. 150, Science 1 Street, Urumqi, Xinjiang 830011, People's Republic of China*

ABSTRACT

We hereby reported a new physical binary cluster (ASCC 19 and ASCC 21) near the Orion star-forming complex based on the data in the literature. Analysis of the results shows that it is likely a primordial binary cluster. The analysis of their member stars with anomalous radial velocities indicates that there is no significant two-body relaxation in this cluster pair, which is also confirmed by their mass segregation results. Moreover, we found that the components of this binary cluster may have been formed by the deep fusion of multiple subclusters based on the analysis of its metal abundances. Finally, we investigated the 3D morphology of this binary cluster, simulated the trajectories of its components in the galactic disk, and concluded that its components may not merge into a single cluster.

Keywords: Galaxy: stellar content — open cluster: ASCC 19 and ASCC 21

1. INTRODUCTION

Open clusters (OCs) that form in the giant molecular clouds are an important part of composing the Milky Way (Lada & Lada 2003). Most of them all survive in isolation in the galactic disk. However, they also live in the Galactic disk as binary, triple, and multiple clusters (e.g. Song et al. 2022; Qin et al. 2023; Li & Zhu 2024) whose proportion is almost comparable to that, about 10% (Bhatia & Hatzidimitriou 1988; Hatzidimitriou & Bhatia 1990) or 12% (Pietrzynski & Udalski 2000), of pairs in the Magellanic Cloud (de La Fuente Marcos & de La Fuente Marcos 2009). The results obtained by (de La Fuente Marcos & de La Fuente Marcos 2009) show that most known binary clusters have very young components (young OCs). Therefore, they are ideal objects used to study and understand the formation and evolution of OCs.

There are several formation channels used to explain the existence of pairs, triplets, or higher multiplicity clusters. First, binary clusters can be formed by tidal capture (van den Bergh 1996). These pairs, not primordial OC binaries, usually share a common motion velocity, with different chemical compositions and ages. Sec-

ond, the resonances of the non-axisymmetric component of the Galactic potential, typically induced by the Galactic bar or spiral arms (e.g. Dehnen 1998; De Simone et al. 2004; Famaey et al. 2005; Chakrabarty 2007), can also result in the formation of double clusters. Third, cluster pairs formed in the same giant molecular cloud at the same time. In this case, they are expected to have similar ages, kinematic characteristics, and chemical composition. The scenario is similar to the simultaneous or primordial formation Fujimoto & Kumai (1997) and Bekki et al. (2004) have elucidated. Finally, double clusters also formed in the sequential formation of OCs. It is well known that supernova shocks or massive stellar winds in one cluster may result in the other one formation out of nearby clouds, then generate a cluster pair (Brown et al. 1995; Goodwin 1997).

There has been a lot of work on the discovery of binary clusters. For example, Pavlovskaya & Filippova (1989) and (Subramaniam et al. 1995) identified 5 possible cluster groups and 18 possible cluster pairs, respectively. After that, de La Fuente Marcos & de La Fuente Marcos (2009) found 34 OC pairs based on the OC samples from NCOVOCC (Dias et al. 2002) and WEBDA (Mermilliod & Paunzen 2003). Conrad et al. (2017) discovered 14 binary clusters from the catalogue provided by Kharchenko et al. (2004, 2005). Recently,

Song et al. (2022) and Li & Zhu (2024) found 14 candidates of truly binary OCs based on the catalog data from Cantat-Gaudin et al. (2020) and 13 newly close binary OCs using the OC catalog of Hunt & Reffert (2023) that were obtained based on Gaia data, respectively. Similarly, Casado (2021) identified 22 new binary or multiple OCs from the catalogs of OCs (Kharchenko et al. 2013; Cantat-Gaudin et al. 2018, 2020; Bica et al. 2019; Liu & Pang 2019; Sim et al. 2019; Castro-Ginard et al. 2020). Then, they (Casado 2021) also found a new binary OC, named Casado 9 and Casado 10, by using Gaia DR2.

Nevertheless, there are many works that reported a set number of new binary OCs, it can still be expected that there are many more new binary clusters in the Milky Way, especially the discovery of primordial binary OCs. The primordial binary OCs may be the final products of multiple mergers of some smaller clusters or stellar groups (de La Fuente Marcos & de La Fuente Marcos 2009). Meanwhile, they also may be potential binary cluster candidates to be merged. Thanks to the precision of Gaia data, there is an opportunity that lets us discover new primordial binary OCs from a newly published catalog of OCs (van Groenigen et al. 2023) taking from the third Gaia Data Release (Gaia DR3) (Gaia Collaboration et al. 2023). With this aim, we searched for all nearby OCs from the OCs catalog published by van Groenigen et al. (2023). We indeed discovered a new primordial OC pair (ASCC 19 and ASCC 21), which was not reported in previous works. The rest of this article is structured as follows: Sect. 2 describes how we selected the data; Sect. 3 presents the results of the primordial OC pair; a summary is presented in Sect. 4.

2. DATA SELECTION

The member stars of ASCC 19 and ASCC 21 were taken from a members' catalog of 2492 OCs published by van Groenigen et al. (2023) on Gaia DR3 data that was obtained by a deep neural network architecture method on the parameter reference of OCs catalog from Cantat-Gaudin et al. (2020) and Castro-Ginard et al. (2022). This catalog has the advantage of providing, as far as possible, the more complete member stars of OCs, since it contains many faint stars (see their Fig. 4), which were not in the previous catalogs. In their catalog, we found that ASCC 19 and ASCC 21 included 3861 and 2709 members, respectively, which are given in Table. 1. The membership probabilities of both member lists are ranging from 0 to 1. In the present study, in order to ensure the reliability of the member stars, we filtered out those members with a probability of less than 1. Therefore, there are 1250 members in ASCC 19 and 998

members in ASCC 21 we obtained where these stars can be regarded as truly members.

3. RESULTS

3.1. Primordial Binary Cluster

The simulations conducted by Bekki et al. (2004) suggested that binary clusters can be formed in cloud-cloud collisions. Initially, when two clouds collide, the intense compression and dissipation of gas will form an elongated molecular cloud. After that, two dense clusters will be formed in the high-density region of the two clouds. As the orbital angular momentum of the two molecular clouds will be transferred to the two clusters, they will begin to evolve around each other (Bekki et al. 2004, see their Fig. 2). If the two molecular clouds have the same properties, such as a metal abundance, Then the binary cluster can be regarded as a primordial binary cluster.

In the present work, we discovered a candidate of the primordial binary cluster (ASCC 19 and ASCC 21) from literature (van Groenigen et al. 2023). Figure 1 shows the member distributions of ASCC 19 and ASCC 21 in a 2D celestial coordinate system, parallax, proper motion, and CMD spaces, meanwhile, there are detailed CMDs for the two OCs in Fig. 2. It was operated and obtained by fitting the isochrones of clusters with 1Myr to 100 Myr, at steps of $\log(\text{age})$ equal to 0.05. Moreover, we used the Gaussian means of the metal abundances from different survey data as the input metallicities for the isochrone fit of the clusters. The fitting function we used in this work is from Eq. 2 of Liu & Pang (2019). By this method, we can obtain the best isochrone fitting lines for our clusters. In addition, we used a step size of 2 times as the error of the best fitting age. We then can see from the two figures that ASCC 19 and ASCC 21 are a truly physical binary cluster because their spatial position is very close to each other, with their proper motion being similar, even the same age ($\log(\text{age}) = 6.95 \pm 0.05$). The related parameters of the cluster pair are listed in Table 1, which also indicates the double cluster is real and reliable.

Due to the proximity and overlap of the two clusters, we performed the crossmatch of the member stars of the two clusters. What we found interesting is that there are 191 member stars from both clusters in the cross-matches. In other words, they belong to both ASCC 19 and ASCC 21. This may imply that there is a gravitational interaction between the inner member stars of the two clusters.

To further verify whether the cluster pair we found is a primordial binary cluster, we should also check their radial velocities (Rv) in addition to checking their ages.

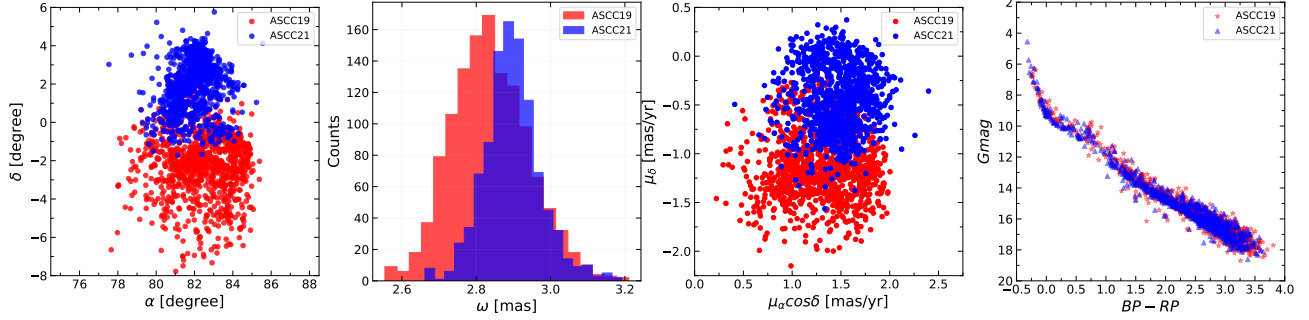


Figure 1. Member distributions of ASCC 19 and ASCC 21 in multi-dimensional parameter space. All members have a membership probability equal to 1. The members of ASCC 19 are marked by red dots or pentagams, with the members of ASCC 21 being represented by blue dots or triangles. Leftmost panel: member distribution of both clusters in a two-dimensional (2D) celestial coordinate system. Middle left panel: histograms of the member stars of both clusters in parallax space. Middle right panel: member distribution of both clusters in proper motion space. Rightmost panel: Color Magnitude Diagram (CMD) of the two clusters. It should be noted that all member data is taken from [van Groenigen et al. \(2023\)](#).

Table 1. Overall parameters of the binary clusters

Parameters	Description	ASCC 19	ASCC 21
α (degree)	Right ascension	82.31 ± 1.07	81.91 ± 0.68
δ (degree)	Declination	-1.89 ± 1.04	1.91 ± 0.96
μ_α ($\text{mas}\cdot\text{yr}^{-1}$)	Proper motion in right ascension	1.34 ± 0.25	1.48 ± 0.17
$\mu_\delta \cos \alpha$ ($\text{mas}\cdot\text{yr}^{-1}$)	Proper motion in declination	-1.12 ± 0.24	-0.44 ± 0.28
ω (mas)	Parallax	2.83 ± 0.07	2.89 ± 0.04
R_v ($\text{km}\cdot\text{s}^{-1}$)	The radial velocity	21.34 ± 4.47	20.05 ± 3.86
[Fe/H] (dex)	The metallic abundance taken from LAMOST-DR11-LRS	-0.16 ± 0.22	-0.15 ± 0.21
[Fe/H] (dex)	The metallic abundance taken from LAMOST-DR11-MRS	-0.14 ± 0.25	-0.12 ± 0.04
[Fe/H] (dex)	The metallic abundance taken from APOGEE-DR17	-0.12 ± 0.06	-0.12 ± 0.07
[Fe/H] (dex)	The metallic abundance taken from GALAH-DR4	-0.36 ± 0.17	-0.40 ± 0.21
Number of all members (-)	the number of members	3861	2709
Number of real members (-)	the number of members with probability = 1	1250	998
X (pc)	The space position along X axis	-301.70 ± 5.42	-306.73 ± 3.48
Y (pc)	The space position along Y axis	-140.17 ± 6.90	-118.23 ± 4.11
Z (pc)	The space position along Z axis	-114.59 ± 5.76	-103.93 ± 5.15
r_h (pc)	The half-mass radius	15.94	11.60
Log(age)	The age of clusters	6.95 ± 0.05	6.95 ± 0.05

Therefore, we plotted the histogram of the radial velocities of these two clusters, as shown in Fig. 3. In order to ensure the reliability of the radial velocity, we restricted the radial velocity of the member stars to be greater than or equal to its three times error. Figure. 3 presents the rectangular distribution of the radial velocity of the double star cluster, which shows the characteristics of centralization and dispersion on both sides. Based on this, we calculated the median of radial velocity and its error for the two clusters, respectively. The distribution over a range of 3 times the median error of the radial velocity is demonstrated within both red boxes in Fig. 3.

We can see that the radial velocities of the two clusters are consistent within the range of their errors, which is also consistent with the motion characteristics of the primordial binary cluster. On the contrary, the member stars not in the two red boxes can be regarded as outlier member stars, especially those with radial velocities above $100 \text{ km}\cdot\text{s}^{-1}$. In the next Section, we conducted an analysis of these outlier member stars.

3.2. Outlier Member Analysis

As those outlier members on the radial velocity parameter may also be truly member stars of the cluster pair, such as the one of [Hu et al. \(2022\)](#), and they

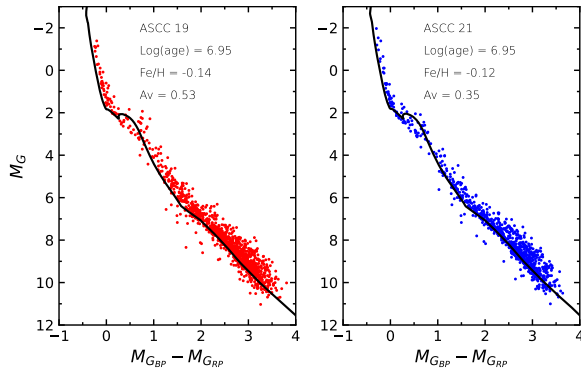


Figure 2. Left panel: CMD of ASCC 19. Right panel: CMD of ASCC 21. The solid black lines are the fitted PARSEC stellar isochrones.

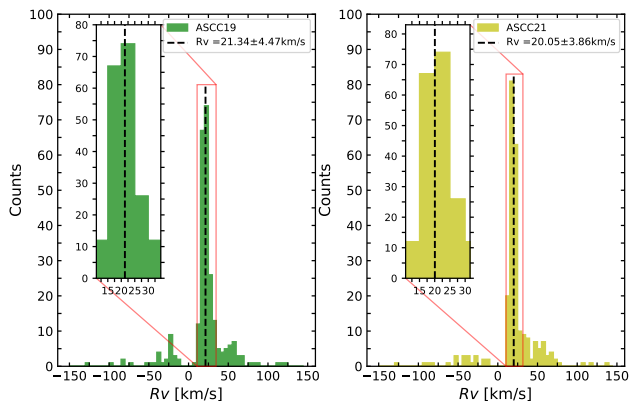


Figure 3. Left panel: radial velocity histogram of ASCC 19. Right panel: radial velocity histogram of ASCC 21. The cluster names, the medians of their radial velocities, and their errors are labeled on the diagram. It should be noted that the ratios of the radial velocities of both clusters to their errors in all radial velocities the diagram presents are more than or equal to 3.

may shed important information on the evolution of the binary cluster, it is necessary to explore them in detail. Figure 4 shows the distribution of member stars of our binary cluster with a ratio of the radial velocity to its error greater than or equal to 3 in four different parameter spaces. Similar to Fig. 1, we still found an overlap of members with radial velocity in the position, parallax, proper motion, and CMD spaces. Moreover, it is apparent in parallax space that the spatial distribution of those outlier member stars runs through the entire internal structure of this binary cluster. Meanwhile, interestingly, most of these outlier member stars are faint stars, which can also be seen as less massive, as shown in the rightmost panel of Fig. 4. Since the outlier member stars have relatively large radial velocities, this may indicate that the two-body relaxation process (e.g., Bergond et al. 2001; Ryon et al. 2017; Mamon et

al. 2019) is underway within the binary cluster. The two-body relaxation leads to the less massive member stars gaining more kinetic energy and gradually moving to the outskirts of clusters, while the more massive member stars lose kinetic energy and thus sink to the center of clusters. Eventually, it may show a mass segregation phenomenon (e.g., Vesperini et al. 2009; Portegies Zwart et al. 2010; Evans & Oh 2022; Noormohammadi et al. 2023).

Further, to explore whether mass segregation occurs in our binary cluster, we adopted the minimum spanning tree method defined by Allison et al. (2009) to quantitatively investigate the mass segregation of these two clusters. Allison et al. (2009) defined the level of mass segregation as the “mass segregation ratio” (Λ_{MSR}). This parameter greater than 1 indicates the signal of mass segregation in clusters. The method also was adopted by Zhang et al. (2020) to diagnose the mass segregation of Blanco 1. The Python code of the mass segregation we adopted in this work is from the `gaia_oc amd` repository published by van Groeningen et al. (2023) on GitHub¹. Figure 5 shows the Λ_{MSR} of ASCC 19 and ASCC 21. We found that ASCC 19 displays a faint signal of mass segregation but ASCC 21 not shows any signal. Combined with the above result that less massive member stars with large radial velocities are distributed throughout the inner space of the binary cluster, this may indicate that the binary cluster is most likely undergoing a two-body relaxation process.

In addition, we also analyzed in detail the outlier member stars with radial velocities exceeding $100 \text{ km}\cdot\text{s}^{-1}$ (colored pentagrams in the rightmost panel of Fig. 4). We found six outlier members with radial velocity over $100 \text{ km}\cdot\text{s}^{-1}$ in the binary cluster, of which four belong to ASCC 19, four belong to ASCC 21, and two belong to both ASCC 19 and ASCC 21. The parameters of the six stars can be seen in Table 2. It is well known that the light variation of stars will affect the measurement of their intrinsic radial velocities. Therefore, It is necessary to check whether these outlier members are variable stars.

We matched and obtained the data of five outlier member stars from the Transiting Exoplanet Survey Satellite (TESS) database. In order to determine whether these member stars are variable stars, we plotted their lightcurves and phase diagrams by the Python package `LightKurve` (Lightkurve Collaboration et al. 2018) and the `PERIOD04` software (Lenz & Breger 2005). Figure 6 presents the lightcurve and phase of

¹ https://github.com/MGJvanGroeningen/gaia_oc amd

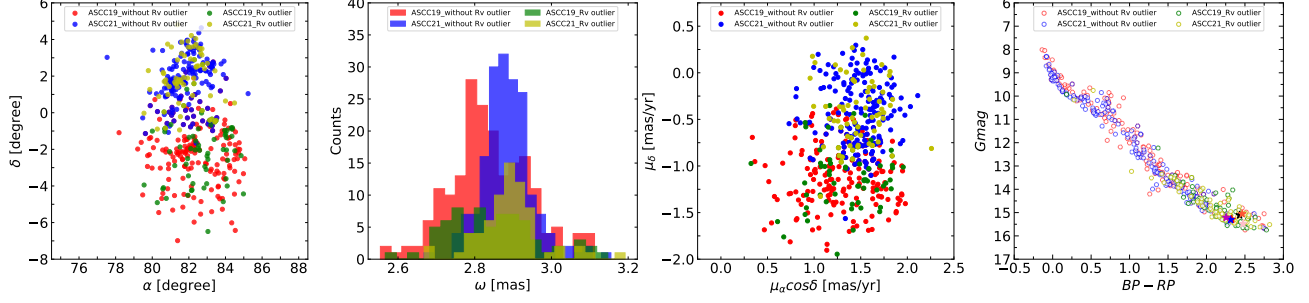


Figure 4. Distributions of members with a ratio of radial velocity to its error more than or equal to 3 of ASCC 19 and ASCC 21 in multi-dimensional parameter space. Leftmost panel: member distribution of both clusters in a 2D celestial coordinate system. Middle left panel: histograms of the member stars of both clusters in parallax space. Middle right panel: member distribution of both clusters in proper motion space. Rightmost panel: Color Magnitude Diagram (CMD) of the two clusters. The pentagrams of different colors represent member stars with outlier radial velocities. The various symbols and their meanings in all panels have been listed in the labels in the corresponding panels.

Table 2. The parameters of outlier members with abnormal radial velocity

(1)	(2)	(3)	(4)	(5)	(6)	(7)	(8)	(9)
Gaia DR3 ID	Ra	Dec	Parallax	Rv	[Fe/H]	TIC ID	Host cluster	Color in Fig. 4
–	(degree)	(degree)	(mas)	(km/s)	(dex)	–	–	–
3220751346266572672	83.14	-0.41	2.842	-126.77 ± 5.71	-0.359 ± 0.070	50788524	ASCC 19 and ASCC 21	Red pentagram
3223872069503741568	82.30	2.89	2.912	117.98 ± 7.80	–	264682835	ASCC 19 and ASCC 21	Blue pentagram
3217579220861913472	84.04	-1.36	2.835	114.34 ± 7.75	-0.081 ± 0.011	427451326	ASCC 19	Purple pentagram
3210550073087799296	82.17	-4.22	2.928	122.30 ± 6.34	–	50587538	ASCC 19	Pink pentagram
3234192596742088192	80.65	1.70	2.934	107.20 ± 6.97	-0.246 ± 0.065	–	ASCC 21	Black pentagram
3223841450681464448	82.43	2.55	2.948	137.78 ± 5.76	-0.133 ± 0.056	264739961	ASCC 21	Coral pentagram

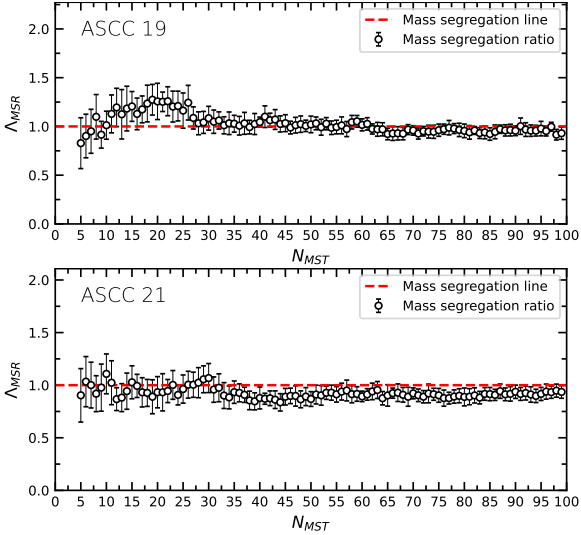


Figure 5. The “mass segregation ratio” (Λ_{MSR}) for ASCC 19 and ASCC 21. N_{MST} denotes the ordinal number of the member stars sorted by G-band magnitude, in sequence from bright to faint.

TIC 264682835 that is one of these outlier members, with a radial velocity of $117.98 \pm 7.80 \text{ km}\cdot\text{s}^{-1}$. It is apparent that this star is a periodic variable star based on its period, which has ever been classified as BY Draconis-type variable star that belongs to rotational

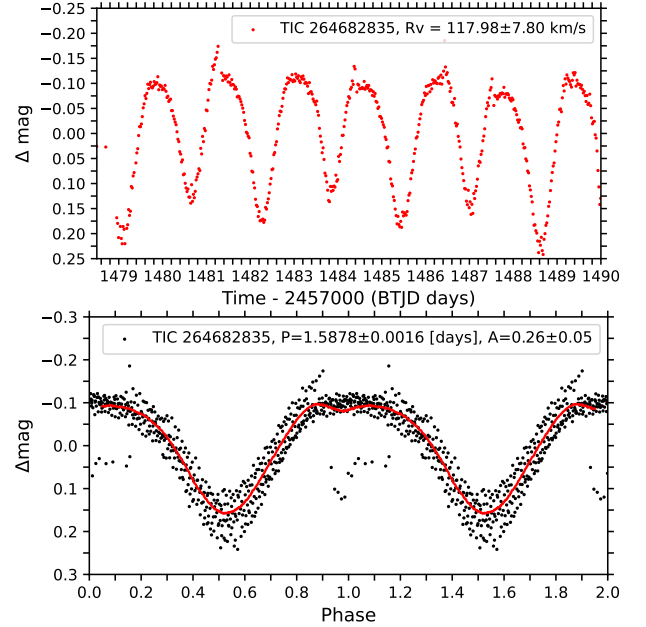


Figure 6. Upper panel: the lightcurve of TIC 264682835. Bottom panel: the phase diagram of TIC 264682835. The red curve represents the fitting curve to the phase. Its radial velocity, period, and amplitude have been labeled in the diagram.

variables (Chen et al. 2020). Chen et al. (2020) pointed

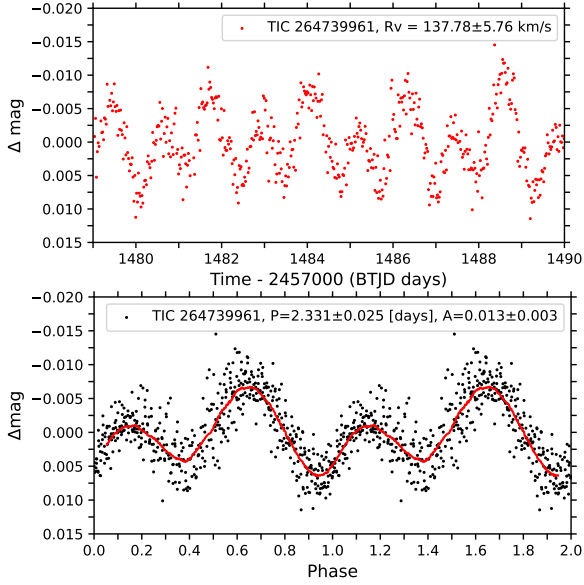


Figure 7. Upper panel: the lightcurve of TIC 264739961. Bottom panel: the phase diagram of TIC 264739961. All symbols are the same as that in Fig. 6

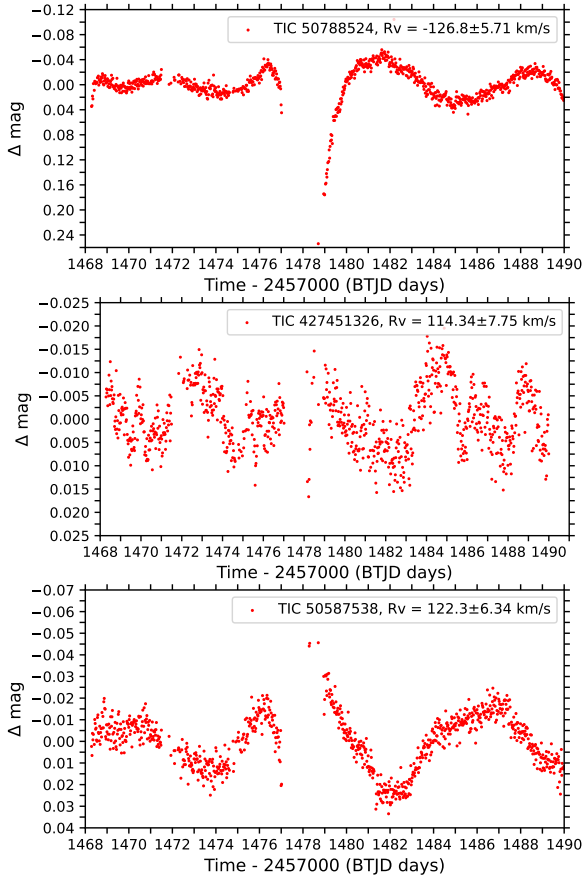


Figure 8. Upper panel: the light curve of TIC 50788524. Middle panel: the light curve of TIC 427451326. Bottom panel: the light curve of TIC 50587538.

out that the rotational periods of BY Draconis-type variables range from 0.25 to 20 days. We found that the period of the object is about 1.5878 ± 0.0016 days which is within the range mentioned above, as shown in Fig. 6. Meanwhile, it is located at the lower edge of the main sequence in CMD of Fig. 4. Tsantaki et al. (2022) published its radial velocity $Rv = 20.418 \pm 0.921$ km·s⁻¹ based on Apache Point Observatory Galactic Evolution Experiment (APOGEE) data. In addition, Using Gaia BP/RP spectra, Verberne et al. (2024) provided its Rv of 302.009 ± 290.928 km·s⁻¹. Since the radial velocity of the star is observed to be variable at different times, combined with its range of light variations, therefore, we deduced that the star may be a variable star. So its radial velocity may not be its systemic radial velocity.

Similarly, we plotted the lightcurve and phase of TIC 264739961, with a radial velocity (Rv) of 137.78 ± 5.76 km·s⁻¹, as shown in Fig. 7. We found that this member is also a periodic variable star, with a period of 2.331 ± 0.025 days and amplitude of 0.013 ± 0.003 mag. Serna et al. (2021) also studied and classified it as a young star, with a projected rotational velocity of 23.3 ± 0.8 km·s⁻¹ based on APOGEE data. Abdurro'uf et al. (2022) published its radial velocity $Rv = 39.20 \pm 0.08$ km·s⁻¹ based on the seventeenth data release of the Sloan Digital Sky Surveys (SDSS-DR17). In addition, there are its radial velocity $Rv = 24.1$ km·s⁻¹ (Ding et al. 2022), $Rv = 19.3 \pm 9.7$ km·s⁻¹ (Zhang et al. 2021) based on the Large Sky Area Multi-Object Fiber Spectroscopic Telescope (LAMOST) data. Tsantaki et al. (2022) reported $Rv = 20.255 \pm 0.355$ km·s⁻¹ for the member based on APOGEE data. Therefore, its radial velocity in this work is not its systemic radial velocity.

Moreover, Fig. 8 shows the light curves of other three outlier stars (TIC 50788524, TIC 427451326, and TIC 50587538). We can find from this picture that these three stars have photometric variations, indicating them to be variable stars. For TIC 50788524, Verberne et al. (2024) reported its $Rv = 110.501 \pm 146.581$ km·s⁻¹. In addition, Abdurro'uf et al. (2022) also gave its Rv (31.946 ± 0.049 km·s⁻¹, 18.038 ± 0.067 km·s⁻¹, and 20.059 ± 0.065 km·s⁻¹) based on APOGEE data. Similarly, TIC 427451326 was also studied by Abdurro'uf et al. (2022) who reported Rv of -5.27 ± 0.008 km·s⁻¹, 43.74 ± 0.06 km·s⁻¹, -4.03 ± 0.05 km·s⁻¹, -5.61 ± 0.06 km·s⁻¹, and 43.63 ± 0.07 km·s⁻¹. Spina et al. (2021), Swiggum et al. (2021), and Tsantaki et al. (2022) published its Rv of 19.98 km·s⁻¹, 20.11 ± 0.02 km·s⁻¹, and 19.97 ± 0.30 km·s⁻¹, respectively. Obviously, like TIC 50788524, the radial velocity of TIC 427451326 in this work is also not its systematic Rv . In addition to

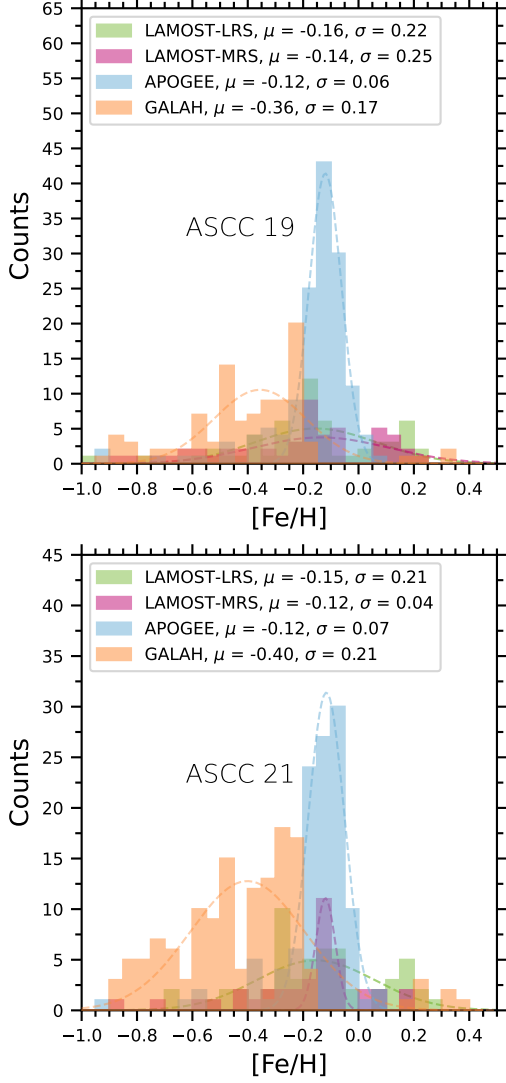


Figure 9. Upper panel: the histograms of the metallicity ($[\text{Fe}/\text{H}]$) of ASCC 19, with the $[\text{Fe}/\text{H}]$ parameters taken from the LRS of LAMOST-DR11 (green), the MRS of LAMOST-DR11 (purple), APOGEE-DR17 (blue), and GALAH-DR4 (yellow), respectively. Bottom panel: the histograms of the metallicity ($[\text{Fe}/\text{H}]$) of ASCC 21, with the $[\text{Fe}/\text{H}]$ parameters taken from the LRS of LAMOST-DR11, the MRS of LAMOST-DR11, APOGEE-DR17, and GALAH-DR4, respectively. The colored dashed lines in the diagram are Gaussian fitting profiles for the metallicities of the two clusters, with their mean and variance being listed in labels.

these two stars, we can also find the R_v parameters of TIC 50587538 from the literature. There is R_v of $-118.73 \pm 158.95 \text{ km}\cdot\text{s}^{-1}$ for this star (Verberne et al. 2024). According to all the parameters above, we can conclude that the radial velocities of these three outlier members are likely not their systemic radial velocities.

3.3. Metallicity

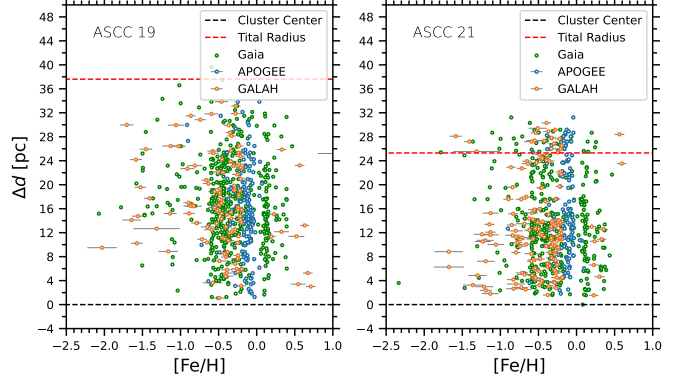


Figure 10. Left panel: the distribution (ASCC 19) between the $[\text{Fe}/\text{H}]$ of the members with metallicity parameters taken from GAIA-DR3 (green), APOGEE-DR17 (blue), and GALAH-DR4 (yellow) and their distances (Δd) to clusters' centers (3D centers). Right panel: the distribution (ASCC 21) between the $[\text{Fe}/\text{H}]$ of the members with metallicity parameters taken from GAIA-DR3, APOGEE-DR17, and GALAH-DR4 and their distances (Δd) to clusters' centers. The black dashed lines in the diagram represent the 3D cluster centers of the two clusters, with their tidal radii being marked by the red dashed lines. The calculation of the tidal radii of the two clusters is detailed in Sec. 3.4.

The member stars of OCs are usually considered to have been born in the same molecular cloud and to have approximately the same metal abundance. In the case of binary clusters, if the two clusters have different metal abundances, then it can be shown that they were not born in the same molecular cloud. Conversely, the fact that they have the same metal abundance would indicate that they were born in the same molecular cloud, which would also indicate that they form a primordial binary cluster. Because except for FGK stars, the metal abundance parameters of other spectral types of stars in Gaia are not reliable, we choose to obtain metal abundance data from other spectrum survey databases by cross-matching. We then obtained 57, 50, 144, and 114 member stars with metal abundance for ASCC 19 from the low-resolution spectrum (LRS) of the eleventh data release of LAMOST (LAMOST-DR11), the medium-resolution spectrum (MRS) of LAMOST-DR11, APOGEE-DR17, and the fourth data release of the Galactic Archaeology with HERMES (GALAH-DR4) and 54, 40, 114, and 140 member stars with metal abundance for ASCC 21 from the LRS of LAMOST-DR11, the MRS of LAMOST-DR11, APOGEE-DR17, and GALAH-DR4, respectively. The metal abundance of these members is greater than or equal to three times its error. We finally plotted the histograms of the metallicities of ASCC 19 and ASCC 21, as shown in Figs. 9. For ASCC 19, its systematic metallicity ($[\text{Fe}/\text{H}]$) includes -0.16 ± 0.22 dex, -0.14 ± 0.25 dex,

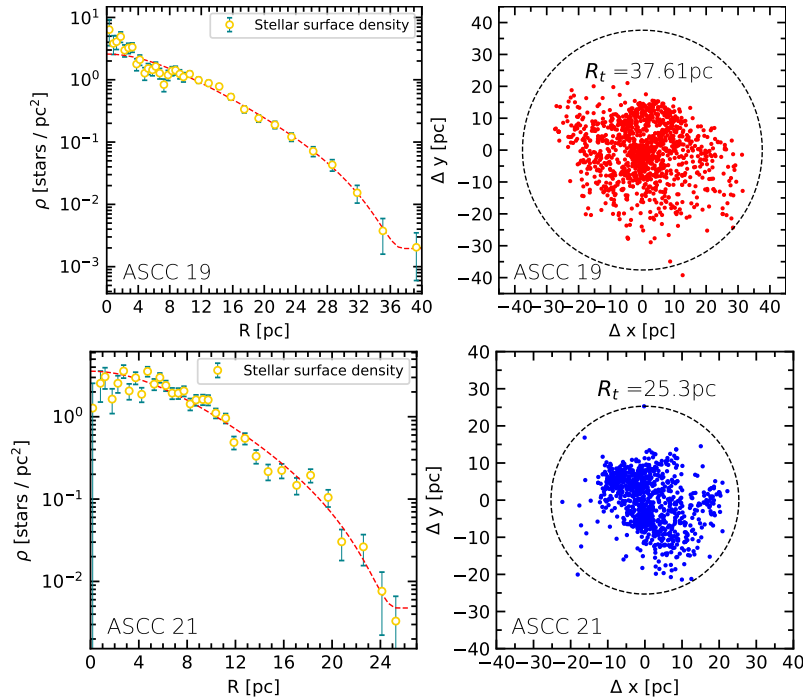


Figure 11. Upper left: the radial density profile of ASCC 19 fitted by King mode. Upper right: distribution of the members (red scatters) of ASCC 19 in two-dimensional space with its circle of tidal radius. Bottom left: the radial density profile of ASCC 21 fitted by King mode. Bottom right: distribution of the members (blue scatters) of ASCC 21 in two-dimensional space with its circle of tidal radius. The tidal radius of ASCC 19 is 37.61 pc, with the one of ASCC 21 being 25.30 pc.

-0.12 ± 0.06 dex, and -0.36 ± 0.17 dex, with the $[\text{Fe}/\text{H}]$ of ASCC 21 being -0.15 ± 0.21 dex, -0.12 ± 0.04 dex, -0.12 ± 0.07 dex, and -0.40 ± 0.21 dex, which were obtained by gaussian fitting. Although the metal abundance of each cluster is not consistent in different surveys, this cluster pair has similar metal abundance in the same survey, implying roughly their same ages. Therefore, we can conclude that the binary cluster consisting of ASCC 19 and ASCC 21 is a primordial cluster pair.

Moreover, Fig. 10 presents the distribution between the $[\text{Fe}/\text{H}]$ of the members with metallicity parameters taken from GAIA-DR3, APOGEE-DR17, and GALAH-DR4 and the distance to clusters' centers for them. We noted that since the metal abundance parameter of Gaia is valid for FGK-type stars, here we only used the metal abundance parameter for the member stars with effective temperatures in the range of 3500 K to 7500 K. How to obtain the distance parameters can be seen in Sec. 3.4. We found that both clusters are roughly composed of member stars with two different metal abundances, as shown in the dispersion distribution on the left and the banded aggregation distribution on the right in the same panel (left or right) for the same survey data (green, or yellow, or blue). This may indicate that the formation of these two clusters may be the result of the merger of multiple subclusters. Meanwhile, this merger is well-mixed and homogeneous because the member stars of

the two metal abundances are distributed in a penetrating pattern from the center of the two clusters to the periphery of the clusters, as shown in Fig. 10. This may be observational evidence that a cluster is formed from a hierarchy of subclusters.

3.4. 3D Spatial Morphology

The study of the morphology of OCs may provide observational evidence for their formation and evolution (Hu et al. 2021a,b). Therefore, we would here make a diagnostic dynamical state for this binary cluster by investigating its morphology.

Since there are 191 member stars that are both members of ASCC 19 and ASCC 21, this suggests that the two clusters have crossed into each other in the 3D space. Therefore, here we investigated the 3D spatial structure of this binary cluster. Meanwhile, it is essential that combing with the tidal radii of the two clusters, we should roughly determine the dynamical state of the binary cluster. In order to get their tidal radii, we adopted the King model (King 1962) to fit their radial density profiles in 2D space, as shown in Fig. 11. The Python code we used in this work was developed by van Groenigen et al. (2023) and is also available in the `gaia_oc_aml` repository on GitHub mentioned above.

Then, we started to obtain the 3D projected distribution of the members of the binary cluster. We thus firstly

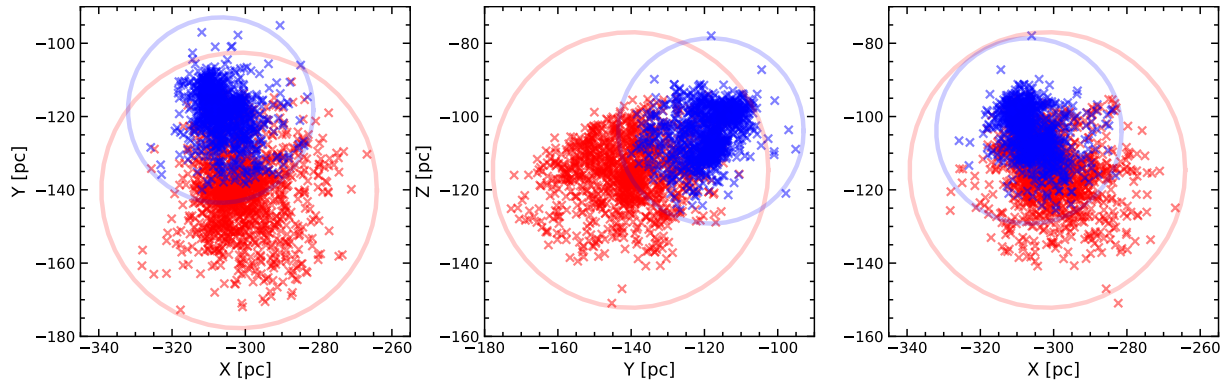


Figure 12. The three-dimensional (3D) projection distribution of the binary cluster on X-Y (left), Y-Z (middle), and X-Z (right) planes. The red and blue crosses indicate the members of ASCC 19 (tidal circle marked by red circle) and ASCC 21 (tidal circle marked by blue circle), respectively.

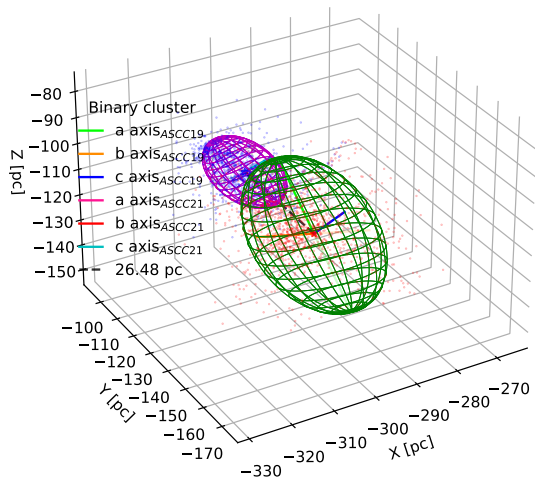


Figure 13. 3D spatial structure of the binary cluster (ASCC 19 and ASCC 21), with ellipsoidal curves. The green ellipsoid with its fitted center (red pentagram) denotes ASCC 19, with the purple ellipsoid with its fitted center (blue pentagram) marking ASCC 21. The small red and blue dots represent the members of ASCC 19 and ASCC 21, respectively. The black dashed line marks the distance between the fitted centers of the two clusters, with 26.48 pc. The different colored bars represent the different axes of the ellipsoids, respectively, as shown in the legend.

calculated their 3D spatial coordinates within the heliocentric Cartesian coordinate system (X , Y , and Z)². The coordinate calculation for each member of the pair was based on the `Python Astropy` package (Astropy Collaboration et al. 2013, 2018). However, because `Gaia`'s par-

² The reference frame is an XYZ Cartesian coordinate system, with the Sun at its center. The positive X-axis is oriented from the Sun's projected position on the Galactic midplane towards the Galactic center, with the positive Y-axis aligning with the direction of the Galactic rotation. The positive Z-axis extends toward the north pole of the Galaxy.

allax has a symmetric error bar, direct inversion of the parallax leads to pseudo-stretching of the cluster's 3D morphology along the line-of-sight direction (see, e.g., Bailer-Jones 2015; Luri et al. 2018; Carrera et al. 2019). We so adopted a Bayesian distance correction model developed by (Carrera et al. 2019; Pang et al. 2021) and used by (Ye et al. 2021; Qin et al. 2023; Hu et al. 2023, 2024) to mitigate this problem. Eventually, we obtained the corrected distances of the members of ASCC 19 and ASCC 21 and further estimated their 3D spatial coordinates. Figure 12 shows the 3D projected morphologies of the binary cluster on the X-Y, Y-Z, and X-Z planes. We found that there is an overlap between the 3D projected distribution of the members of the two clusters, as well as their tidal circles. Therefore, we speculated that there is some gravitational interaction between them, and then there may be a tendency to merge.

Next, we fitted a 3D ellipsoid to the 3D spatial distribution of the member stars of ASCC 19 and ASCC 21, a method that has also been adopted by Hu et al. (2024). Figure 13 displays the 3D spatial structure of this binary cluster, as well as the 3D fitting ellipsoids of its components. Like to the result in Fig. 12, there is also a crossover in their 3D fitting ellipsoids. In addition, we found that the distance between the centers of the fitted ellipsoids of ASCC 19 and ASCC 21 is approximately half the sum of their tidal radii. This also indicates that the pair may be undergoing a merger process.

3.5. Predicting Motion Trajectories

In order to verify whether ASCC 19 and ASCC 21 will merge into a cluster, we simulated their motion orbits using the `galpy.potential` module (MWPotential2014) within the `Python galpy` (Bovy 2015) package. It is an axisymmetric potential module that is composed of a Miyamoto-Nagai disc (Miyamoto & Nagai 1975), a bulge, and a dark matter halo modeled with a Navarro-Frenk-White (NFW) potential (Navarro

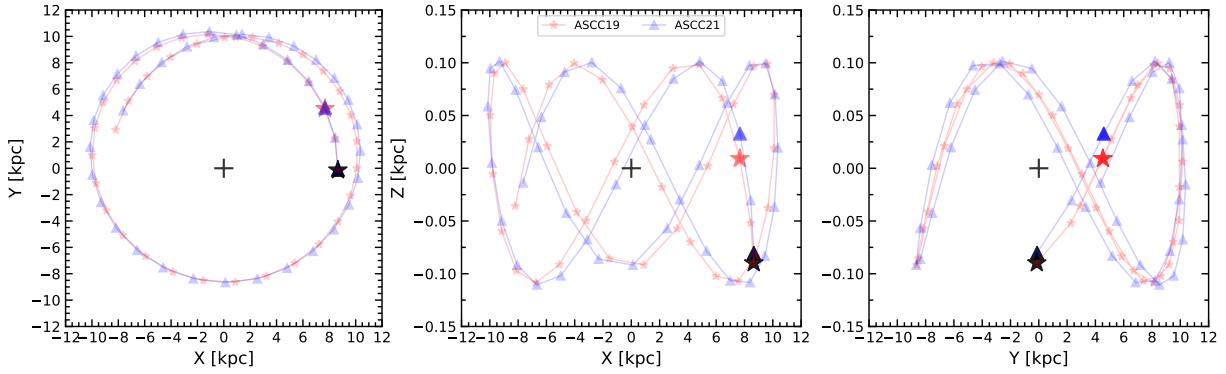


Figure 14. The 3D projected motion trajectories of ASCC 19 and ASCC 21 on the X-Y (left), Y-Z (middle), and X-Z (right) planes. The positions marked by black pentagram (ASCC 19) and triangle (ASCC 21) are now where they are, with their positions after 40 Myr being denoted by red pentagram (ASCC 19) and blue triangle (ASCC 21). The time span between two neighboring symbol marker points is 20 Myr for both red and blue trajectories.

et al. 1997). By inputting the position, parallax, proper motion, and radial velocity parameters of ASCC 19 and ASCC 21 into the module, we integrated the potential module and obtained the 3D spatial motion trajectories of these two clusters forward.

Figure 14 presents the projected motion trajectories of the two clusters on the X-Y (left), Y-Z (middle), and X-Z (right) planes within 400 Myr forward. We can see that this double cluster orbits roughly one and a half revolutions in the galactic disk within 400 Myr. They are now at the positions marked by black pentagram (ASCC 19) and triangle (ASCC 21) in the galactic disk. After 40 Myr, they will appear in the positions denoted by red pentagram (ASCC 19) and blue triangle (ASCC 21), as shown in Fig. 14. Therefore, it is possible that ASCC 19 and ASCC 21 will not merge a cluster as time passes based on this simulation for their motion orbits within `galpy` frame.

4. SUMMARY

Based on data from the literature, we discovered and confirmed for the first time that the combination of ASCC19 and ASCC21 is a physical binary cluster from the parameter spaces of 2D celestial coordinate system position, proper motion, parallax, and CMD. Meanwhile, Based on the analysis of its metal abundance, we are confident that it is a primary binary cluster.

In addition, obtaining photometric data from TESS, combined with radial velocity parameters published in the literature, we then inspected its radial velocity anomalies stars and found that they are variable stars. Therefore, their radial velocities in this work are not systemic radial velocities.

Next, we performed an in-depth analysis of the metal abundances in the binary cluster and found that the components in the binary cluster are all formed by deep homogeneous mixing of subclusters.

Finally, we also performed a 3D morphological analysis of the binary cluster and found that there is a tendency for the components in the binary cluster to merge into a single cluster. However, based on our simulated orbital analysis of the components using `galpy` package, they will not merge into a cluster in the future but continue along similar orbits.

ACKNOWLEDGMENTS

This work is supported by the National Natural Science Foundation of China (NSFC) under grant 12303037, the Fundamental Research Funds of China West Normal University (CWNU, No.493065), the National Key R&D Program of China (Nos. 2021YFA1600401 and 2021YFA1600400), the National Natural Science Foundation of China (NSFC) under grant 12173028, the Chinese Space Station Telescope project: CMS-CSST-2021-A10, the Sichuan Youth Science and Technology Innovation Research Team (Grant No. 21CXTD0038), and the Innovation Team Funds of China West Normal (No. KCXTD2022-6). Qingshun Hu would like to acknowledge the financial support provided by the China Scholarship Council program (Grant No. 202308510136). This study has made use of the Gaia DR3, operated by the European Space Agency (ESA) space mission (Gaia). The Gaia archive website is <https://archives.esac.esa.int/gaia/>. The TESS data presented in this paper were obtained from the Mikulski Archive for Space Telescopes (MAST) at the Space Telescope Science Institute (STScI). STScI is operated by the Association of Universities for Research in Astronomy, Inc., under NASA contract NAS5-26555. Some of the radial velocities this work adopted are based on the data acquired through the Guoshoujing Telescope. Guoshoujing Telescope (the Large Sky Area Multi-Object Fiber Spectroscopic Telescope; LAMOST) is a National Major Scientific Project built by the Chinese Academy of Sciences. LAOMST is operated and managed by the National Astronomical Observatories, Chinese Academy of Sciences. This work also adopted the data from the Galactic Archaeology with HERMES (GALAH) survey. Software: **Astropy** (Astropy Collaboration et al. 2018), **Galpy** (Bovy 2015), **LightKurve** (Lightkurve Collaboration et al. 2018), and **TOPCAT** (Taylor 2005).

REFERENCES

- Abdurro'uf, Accetta, K., Aerts, C., et al. 2022, *ApJS*, 259, 35.
- Allison, R. J., Goodwin, S. P., Parker, R. J., et al. 2009, *MNRAS*, 395, 1449.
- Astropy Collaboration, Price-Whelan, A. M., Sipőcz, B. M., et al. 2018, *AJ*, 156, 123.
- Astropy Collaboration, Robitaille, T. P., Tollerud, E. J., et al. 2013, *A&A*, 558, A33
- Bailer-Jones, C. A. L. 2015, *PASP*, 127, 994
- Bekki, K., Beasley, M. A., Forbes, D. A., et al. 2004, *ApJ*, 602, 730.
- Bergond, G., Leon, S., & Guibert, J. 2001, *A&A*, 377, 462.
- Bhatia, R. K. & Hatzidimitriou, D. 1988, *MNRAS*, 230, 215.
- Bica, E., Pavani, D. B., Bonatto, C. J., et al. 2019, *AJ*, 157, 12.
- Bovy, J. 2015, *ApJS*, 216, 29.
- Brown, J. H., Burkert, A., & Truran, J. W. 1995, *ApJ*, 440, 666.
- Carrera, R., Pasquato, M., Vallenari, A., et al. 2019, *A&A*, 627, A119
- Cantat-Gaudin, T., Jordi, C., Vallenari, A., et al. 2018, *A&A*, 618, A93.
- Cantat-Gaudin, T., Anders, F., Castro-Ginard, A., et al. 2020, *A&A*, 640, A1.
- Castro-Ginard, A., Jordi, C., Luri, X., et al. 2022, *A&A*, 661, A118.
- Casado, J. 2021, *Astronomy Reports*, 65, 755.
- Casado, J. 2021, *Research in Astronomy and Astrophysics*, 21, 117.
- Castro-Ginard, A., Jordi, C., Luri, X., et al. 2020, *A&A*, 635, A45.
- Chen, X., Wang, S., Deng, L., et al. 2020, *ApJS*, 249, 18.
- Conrad, C., Scholz, R.-D., Kharchenko, N. V., et al. 2017, *A&A*, 600, A106
- Chakrabarty, D. 2007, *A&A*, 467, 145.
- de La Fuente Marcos, R. & de La Fuente Marcos, C. 2009, *A&A*, 500, L13.
- Dehnen, W. 1998, *AJ*, 115, 2384.
- De Simone, R., Wu, X., & Tremaine, S. 2004, *MNRAS*, 350, 627.
- Dias, W. S., Alessi, B. S., Moitinho, A., et al. 2002, *A&A*, 389, 871.
- Ding, M.-Y., Shi, J.-R., Wu, Y., et al. 2022, *ApJS*, 260, 45.
- Evans, N. W. & Oh, S. 2022, *MNRAS*, 512, 3846.
- Famaey, B., Jorissen, A., Luri, X., et al. 2005, *A&A*, 430, 165.
- Fujimoto, M. & Kumai, Y. 1997, *AJ*, 113, 249. doi:10.1086/118249
- Gaia Collaboration, Vallenari, A., Brown, A. G. A., et al. 2023, *A&A*, 674, A1.
- Goodwin, S. P. 1997, *MNRAS*, 284, 785.
- Hatzidimitriou, D. & Bhatia, R. K. 1990, *A&A*, 230, 11
- Hu, Q., Zhang, Y., Esamdin, A., et al. 2021, *ApJ*, 912, 5
- Hu, Q., Zhang, Y., & Esamdin, A. 2021, *A&A*, 656, A49
- Hu, Q., Zhang, Y., Esamdin, A., et al. 2022, *ApJ*, 935, 142
- Hu, Q., Zhang, Y., Esamdin, A., et al. 2023, *A&A*, 672, A12
- Hu, Q., Zhang, Y., Qin, S., et al. 2024, *A&A*, 687, A291
- Hunt, E. L. & Reffert, S. 2023, *A&A*, 673, A114.
- Kharchenko, N. V., Piskunov, A. E., Röser, S., et al. 2004, *Astronomische Nachrichten*, 325, 740.
- Kharchenko, N. V., Piskunov, A. E., Röser, S., et al. 2005, *A&A*, 440, 403.
- Kharchenko, N. V., Piskunov, A. E., Schilbach, E., et al. 2013, *A&A*, 558, A53
- King, I. 1962, *AJ*, 67, 471.
- Lada, C. J. & Lada, E. A. 2003, *ARA&A*, 41, 57.
- Lenz, P. & Breger, M. 2005, *Communications in Asteroseismology*, 146, 53.
- Li, Z. & Zhu, Z. 2024, arXiv:2405.02530.
- Lightkurve Collaboration, Cardoso, J. V. de M., Hedges, C., et al. 2018, *Astrophysics Source Code Library*. ascl:1812.013
- Liu, L. & Pang, X. 2019, *ApJS*, 245, 32.
- Luri, X., Brown, A. G. A., Sarro, L. M., et al. 2018, *A&A*, 616, A9
- Mamon, G. A., Cava, A., Biviano, A., et al. 2019, *A&A*, 631, A131.
- Mermilliod, J.-C. & Paunzen, E. 2003, *A&A*, 410, 511.
- Miyamoto, M. & Nagai, R. 1975, *PASJ*, 27, 533
- Navarro, J. F., Frenk, C. S., & White, S. D. M. 1997, *ApJ*, 490, 493.
- Noormohammadi, M., Khakian Ghomi, M., & Haghi, H. 2023, *MNRAS*, 523, 3538.
- Pang, X., Li, Y., Yu, Z., et al. 2021, *ApJ*, 912, 162
- Pavlovskaya, E. D. & Filippova, A. A. 1989, *Soviet Ast.*, 33, 6
- Portegies Zwart, S. F., McMillan, S. L. W., & Gieles, M. 2010, *ARA&A*, 48, 431.
- Pietrzynski, G. & Udalski, A. 2000, *AcA*, 50, 355.
- Qin, M. F., Zhang, Y., Liu, J., et al. 2023, *A&A*, 675, A67.
- Ryon, J. E., Gallagher, J. S., Smith, L. J., et al. 2017, *ApJ*, 841, 92.
- Serna, J., Hernandez, J., Kounkel, M., et al. 2021, *ApJ*, 923, 177.
- Song, F., Esamdin, A., Hu, Q., et al. 2022, *A&A*, 666, A75.
- Spina, L., Ting, Y.-S., De Silva, G. M., et al. 2021, *MNRAS*, 503, 3279.

- Sim, G., Lee, S. H., Ann, H. B., et al. 2019, *Journal of Korean Astronomical Society*, 52, 145.
- Subramaniam, A., Gorti, U., Sagar, R., et al. 1995, *A&A*, 302, 86
- Swiggum, C., D’Onghia, E., Alves, J., et al. 2021, *ApJ*, 917, 21.
- Taylor, M. B. 2005, *Astronomical Data Analysis Software and Systems XIV*, 347, 29
- Tsantaki, M., Pancino, E., Marrese, P., et al. 2022, *A&A*, 659, A95.
- van den Bergh, S. 1996, *ApJL*, 471, L31.
- van Groeningen, M. G. J., Castro-Ginard, A., Brown, A. G. A., et al. 2023, *A&A*, 675, A68.
- Verberne, S., Koposov, S. E., Rossi, E. M., et al. 2024, *A&A*, 684, A29.
- Vesperini, E., McMillan, S. L. W., & Portegies Zwart, S. 2009, *ApJ*, 698, 615.
- Ye, X., Zhao, J., Zhang, J., et al. 2021, *AJ*, 162, 171
- Zhang, Y., Tang, S.-Y., Chen, W. P., et al. 2020, *ApJ*, 889, 99.
- Zhang, L.-yun., Meng, G., Long, L., et al. 2021, *ApJS*, 253, 19.